World Journal of Advanced Research and Reviews
eISSN: 2581-9615 CODEN (USA): WJARAI
Cross Ref DOI: 10.30574/wjarr
Journal homepage: https://wjarr.com/

(RESEARCH ARTICLE)

Check for updates

Application of bio-synthesized silicon nanoparticles from bamboo stem for the remediation of heavy metals in contaminated water

Nsikak Bassey Essien [1, *], Nnabuk Okon Eddy [2], Ukeme N.Essien [3], Idongesit Akpan James [4] and Deborah O Josiah [5]

[1] *Department of Science Laboratory Technology, School of Applied Sciences, Federal Polytechnic Ukana, Ikot Ekpene, Akwa Ibom State, Nigeria.*
[2] *Department of Chemistry, Faculty of Physical Sciences, University of Nigeria, Nsukka, Nigeria.*
[3] *Department of forestry and wildlife, Faculty of Agriculture, University of uyo, Akwa Ibom State, Nigeria.*
[4] *Department of science Laboratory Technology, School of Applied Sciences, Akwa Ibom State polytechnic, Ikot Osurua, Ikot Ekpene, Akwa Ibom State, Nigeria.*
[5] *Department of Chemistry, faculty of natural and applied Sciences, University of Illorin, Kwara state, Nigeria.*

World Journal of Advanced Research and Reviews, 2026, 29(03), 1354-1371

Publication history: Received on 09 February 2026; revised on 16 March 2026; accepted on 18 March 2026

Article DOI: https://doi.org/10.30574/wjarr.2026.29.3.0586

Abstract

Silicon nanoparticles (SiONPs) were successfully synthesized from bamboo stem for the remediation of Pb (II), Cr (VI) and Cd (II) ions in contaminated water, the synthesized SiONPs was found to be an excellent adsorbent for Pb (II) ions as compared to Cr (VI) and Cd (II) ions. The investigation to determine the adsorption efficiency of SiONPs from bamboo stem for the removal of Pb (II), Cr (VI) and Cd (II) ions was carried out using batch process in aqueous solution. The after-adsorption characterization of the SiONPs through FTIR, XRD, UV-VIS and XRF indicated strong evidence of interaction that can be attributed to the binding of the heavy metal's ions to the surface of the adsorbent. The adsorption of these metal ions from aqueous solution is consistent with the mechanism of physical adsorption; it is time independent, concentration and adsorbent dose dependent. Its adsorption characteristics best fitted the Freundlich, Temkin and Dubinin-Radushkevich adsorption models. From the Freundlich and Temkin models, the extent of interaction was established through the values of their respective adsorption constant. Also, the adsorption kinetic of the adsorbates agrees excellently with the pseudo first and second order kinetic models.

Keywords: Heavy Metal Pollutants (HMPs); Water; Pb (II); Cr (VI) And Cd (II) Ions; Adsorption; SiONPs and Bamboo Stem

1. Introduction

The Nigerian environment is currently going through diverse levels of contamination arising from industrial, agricultural, domestic, mining and other sources.[1]This implies that the public health of our environment is under severe threat and the future consequences may negatively impact the aquatic and terrestrial ecosystem.[2]Several studies have confirmed that the most impacted component of the environment is the aquatic ecosystem[3] because of the high level of dependence of other components on water, the increasing volume of industrial waste, anthropogenic activities, the high migration rate of water through surface runoff, absorption and other routes[4] has increased the level of heavy metals pollution through bio magnification. Heavy metal ions whose densities are above 5 g/cm^3 are always released into the environment through both natural and anthropogenic activities[5,6,7]during the process of contamination. Most of these metal ions like Hg(II), Cr(II), Cr(VI), Ni(II), Cd(II), Pb(II), Se(II) and As(II) ions etc, originate from less of a natural phenomenon but mostly from various anthropogenic activities of man. The natural sources of HMPs into the

* Corresponding author: Nsikak Bassey Essien

environments are from rocks (sedimentary, metamorphic, and igneous rocks) through their interactions with the environment during leaching, erosion, weathering, soil formation etc,[9] they are being transported and distributed further into the environment through ground water(streams, springs, lakes, and rivers), these ground water can also naturally transport HMPs over a considerable distance and its chemical composition varies from location to location depending on the geological features of where it runs through, other features that can contribute to the identity of HMPs in a particular location includes the chemical, biological and physical activities such as dilution and evaporation, redox potential, pH, temperature and living organism,[6]. HMPs carried by water can be absorbed either by oxy-hydroxides or aquatic organism like algae which introduces it to the food chain, they quickly accumulate in living organism through various processes like the food chains,[10], they are found to be very toxic, persistent, non-biodegradable and this leads to extensive pollution of the land, water and air thereby causing several severe adverse health defects like cancer,[11] skin irritation, lungs and liver damage,[12]renal failure,[13] Oxidative stress, brain damage,[14] cramps convulsion [15] etc.

Therefore, remediation, detection and removal of HMPs from wastewater is drawing so much attention because of these adverse effects they pose. [6] The remediation and removal of heavy metals in an environment is an analytical method that has been used to alleviate environmental issues, contributes to knowledge in biomedical studies,[16] tackle global security concerns and make our environment green again. .[17]

Plant waste from agricultural activities can be turned into good use if properly harnessed. Developing and transition countries are often faced with land contamination and pollution problems from this plant waste and these can be turned to become useful tools for the remediation of heavy metals and dyes in contaminated water. Bamboo trees are economic tree plants found both in developing and developed countries, bamboo trees is mainly planted to be used as a building material during construction,[18] the stems of bamboo are often disposed of indiscriminately and as such they often lead to land pollution due to its occupation. However, silicon nanoparticles can be biosynthesized from this plant waste for the remediation of heavy metals in contaminated water, by this approach, we will be able to solve two environmental problems which include reducing plant waste occupation and reduction/remediation and sensing of heavy metals pollutants in aqueous environment.[19]

2. Materials and Methods for the synthesis of sinps

Samples of bamboo were collected from Ikot Ekpene L.G.A in Akwa Ibom State, where they were disposed as waste. The samples were dried to constant weight under the sun. The moisture free samples were crushed to powdered formed and re-dried. After drying, they were reacted with 2M hydrochloric acid (in the ratio of 4:1) to produce silicon chloride and hydrogen (equation 1). The product was washed with distilled water severally to remove unreacted acid. The washed samples were re-dried in the oven to constant weight, after which it was made to react with 50% sodium hydroxide to produce SiO_2 and sodium chloride (equation 2). After washing and drying, the resulting product (SiO_2) was calcined at 800°C in a muffle furnace for 3 hours to form silicon oxide nanoparticles (SiONPs)

$$HCl + Si \rightarrow SiCl_4 + 2H_2 \quad \text{equation 1}$$

$$SiCl_4 + 4NaOH \rightarrow SiO_2 + 4NaCl + 2H_2O \qquad equation\ 2$$

$$SiO_2 \frac{800°C}{3Hrs, \Delta} \rightarrow SiONP$$

The produced SiONPs were characterized using XRD, FTIR, SEM-EDX, XRF and UV-VIS spectroscopic techniques.

2.1. Pre-characterization. Of synthesized SiONPs from Bamboo

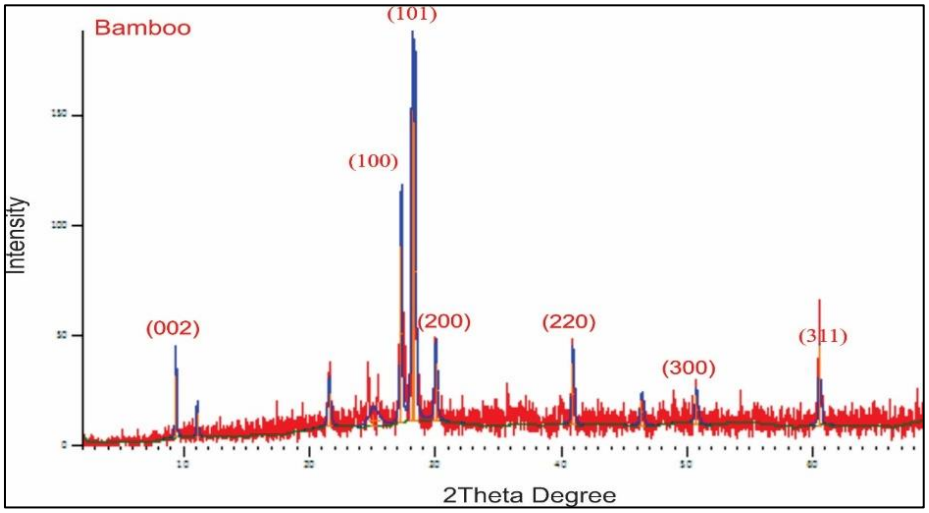

Figure 1 X-ray diffraction pattern of SiONPs produced from Bamboo

Table 1 Diffraction parameters deduced from the XRD pattern SiONPs derived from Bamboo

Pos. [°2Th.]	Height [cts]	FWHM Left [°2Th.]	d-spacing [Å]	Rel. Int. [%]
9.4063	28.72	0.1181	9.40243	20.24
11.1106	11.46	0.1181	7.96366	8.08
21.5881	15.71	0.2362	4.11651	11.07
25.1117	5.74	0.9446	3.54632	4.04
27.2868	81.02	0.1574	3.26837	57.09
28.1415	141.92	0.1378	3.17102	100.00
28.3868	135.96	0.1181	3.14417	95.80
30.0399	26.52	0.2362	2.97481	18.69
40.9277	28.57	0.1968	2.20510	20.13
46.4041	11.65	0.2362	1.95682	8.21
50.7297	13.18	0.2362	1.79965	9.29
60.5015	36.26	0.1181	1.53029	25.55

2.2. XRD analysis

The X-ray diffraction (XRD) pattern of the silicon-enriched bamboo-based adsorbent was recorded using Cu Kα radiation (λ = 1.5406 Å) over a 2θ range of 2–70°. The diffractogram confirms the successful incorporation of silicon-based nanoparticles within the bamboo matrix, yielding a structurally heterogeneous composite suitable for heavy-metal adsorption.

The most intense reflection at 2θ ≈ 28.1–28.4° (d ≈ 3.14–3.17 Å) is indexed to the (101) plane of crystalline silicon/silica, indicating that silicon-based phases constitute the dominant crystalline component. The sharp and high-intensity nature of this peak suggests good crystallinity and nanoscale ordering, which favor the formation of reactive silanol (Si–OH) groups that facilitate surface complexation and ion-exchange mechanisms. Additional reflections at 2θ ≈ 27.3° (100), 30.0° (200), 40.9° (220), 50.7° (300), and 60.5° (311) further confirm the presence and structural integrity of crystalline silicon nanoparticles, implying effective dispersion within the bamboo matrix and minimal agglomeration.

A low-angle peak at 2θ ≈ 9.4°, corresponding to the (002) plane of cellulose, indicates partial retention of the native bamboo microfibrillar structure. However, its comparatively lower intensity suggests partial disruption of organic crystallinity, which may enhance pore accessibility and metal-ion diffusion. The broad diffuse halo observed between 15–25° is attributed to amorphous lingo-cellulosic components and amorphous silica, contributing to surface heterogeneity and porosity that support and improved adsorption kinetics and capacity.

Overall, the XRD results demonstrate that the synthesized material is a silicon-rich, semi-crystalline bamboo-based composite integrating crystalline silicon nanoparticles within an amorphous lingo-cellulosic framework. This synergistic structural configuration provides abundant active sites, enhanced porosity, and structural stability, supporting its potential effectiveness in heavy-metal remediation from aqueous systems.

2.3. SEM-EDX analysis

The combined SEM–EDX analysis (Figure. 2) provides detailed information on the morphology and elemental composition of the synthesized SiONPs. SEM micrographs (Figure. 2) reveal a heterogeneous surface characterized by irregularly shaped particles with rough and porous textures. Such morphological features are favorable for adsorption, as they increase surface area, enhance the availability of active sites, and facilitate effective interaction between the adsorbent and target metal ions.

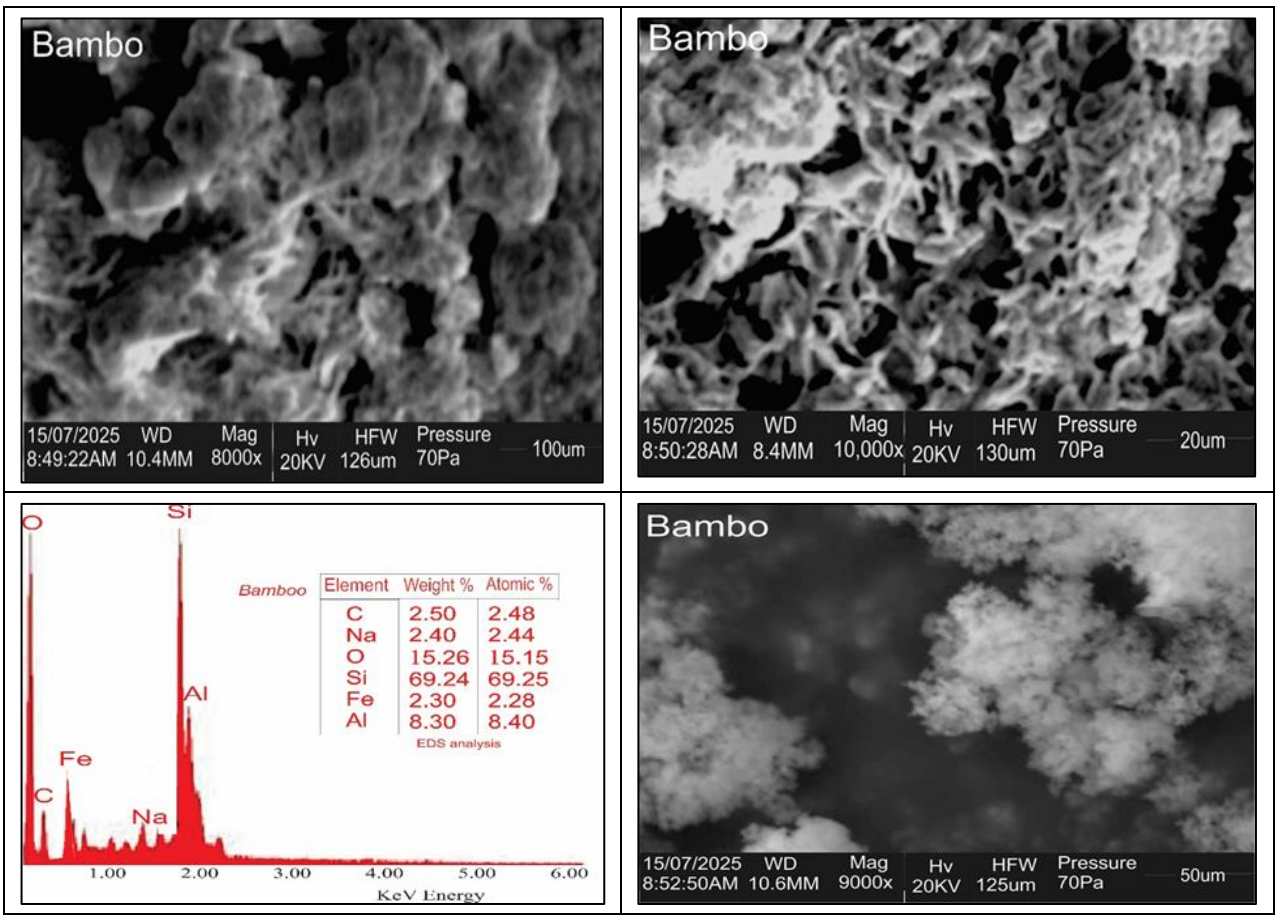

Figure 2 SEM-EDX result of SiONPs produced from Bamboo

EDX results confirm the predominance of silicon (69.24 wt%; 69.25 at%) with oxygen as the second most abundant element (15.26 wt%; 15.15 at%), consistent with the formation of silicon oxide-based nanoparticles. The close agreement between weight and atomic percentages indicates good compositional uniformity and successful synthesis of silicon-rich nanoparticles. The homogeneous distribution of these elements further suggests material consistency.

The detectable presence of calcium may be attributed to precursor composition or intentional modification during synthesis, potentially influencing surface chemistry and adsorption performance. Aluminium was also identified in minor amounts, likely arising from residual impurities introduced during processing. Overall, the SEM–EDX results

confirm the successful synthesis of homogeneous, silicon-dominant nanoparticles with surface characteristics suitable for adsorption applications.

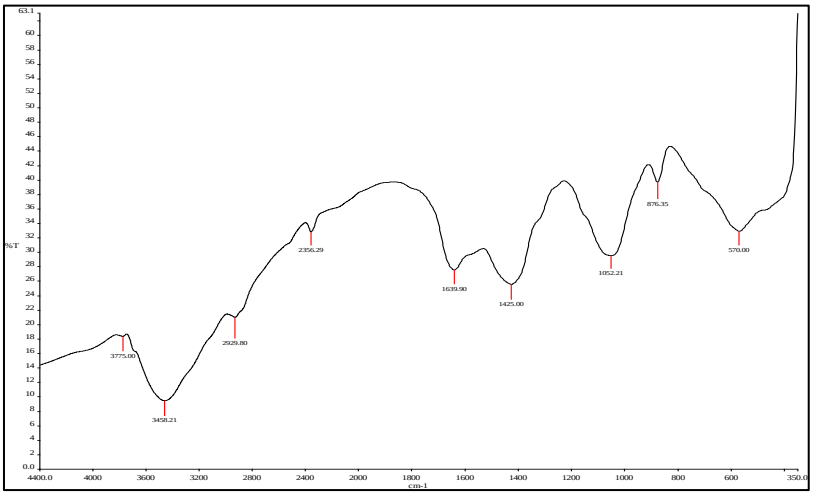

Figure 3 FTIR result of SiONPs produced from Bamboo

2.4. FTIR analysis

FTIR analysis (Shimadzu FTIR-8400S) of the bamboo-derived silicon nanoparticles prior to adsorption (Figure. 3) confirms the formation of a silica-rich nanostructure with abundant surface-active functionalities. A broad band at ~3400–3450 cm^{-1} is assigned to O–H stretching of silanol (Si–OH) groups and adsorbed water, indicating the presence of primary adsorption sites responsible for hydrogen bonding, electrostatic attraction, and surface complexation.

A weak band at ~2920–2950 cm^{-1} corresponds to aliphatic C–H stretching, suggesting minimal residual organic content and dominance of the inorganic framework. The band at ~1700–1720 cm^{-1} is attributed to C=O stretching of carbonyl/carboxyl groups, which can enhance metal binding through chelation. The ~1600–1630 cm^{-1} band arises from H–O–H bending of adsorbed water, reflecting the hydrophilic nature of the material.

The most intense band at ~1050–1100 cm^{-1} corresponds to asymmetric Si–O–Si stretching, confirming a well-developed siloxane network, while bands below ~800 cm^{-1} are assigned to Si–O symmetric stretching and bending vibrations. Overall, the spectrum verifies successful synthesis of stable, silica-based nanoparticles with functional groups suitable for heavy-metal adsorption.

Table 2 XRF profiling for the oxide composition of the SiONPs from Bamboo

Sample	SiO_2	Al_2O_3	Fe_2O_3	MnO	CaO	P_2O_5	K_2O	TiO_2	MgO	Na_2O	LOI	Ba	Ce	Rb	Cd	Cr	Cu	Cd	Pb
Bamboo	52.54	30.44	3.59	0.01	1.54	0.01	0.27	1.19	0.05	0.02	0.50	0.37	4.6	0.32	Nd	0.85	0.05	0.10	0.10

2.5. XRF analysis

X-ray fluorescence (XRF) analysis (Table 2) was conducted to determine the chemical composition and purity of bamboo-derived silicon nanoparticles. The results confirm a silica-dominant material, with SiO_2 constituting 52.54 wt%, verifying the effective conversion of bamboo into a silicon-rich nanostructure. The high silica content indicates a stable siliceous framework with abundant surface silanol (Si–OH) groups, which serve as active sites for metal-ion complexation in aqueous systems.

Al_2O_3 (30.44 wt%) represents a significant secondary component, suggesting the formation of aluminosilicate phases. The incorporation of alumina may introduce negatively charged sites and structural defects within the silica network, thereby enhancing affinity toward cationic heavy metals while improving thermal and mechanical stability. Fe_2O_3 (3.59 wt%), present in minor quantity, may contribute redox-active sites and support surface complexation, particularly in chromium-related remediation processes.

Additional oxides, including TiO_2 (1.19 wt%), CaO (1.54 wt%), and trace amounts of K_2O, MgO, and Na_2O, act as structural modifiers influencing surface charge and ion-exchange behavior. The low loss on ignition (0.50 wt%) indicates minimal residual organic matter, reflecting effective thermal treatment while retaining functional surface groups beneficial for adsorption.

Trace heavy metals (Cr, Cu, Cd, and Pb) were detected at negligible ppm levels, confirming high elemental purity and suitability for water treatment applications without risk of secondary contamination. Overall, the XRF results demonstrate that the synthesized nanoparticles are silicon-rich, structurally stable, and chemically active, supporting their applicability in heavy-metal remediation.

2.6. UV-VIS studies

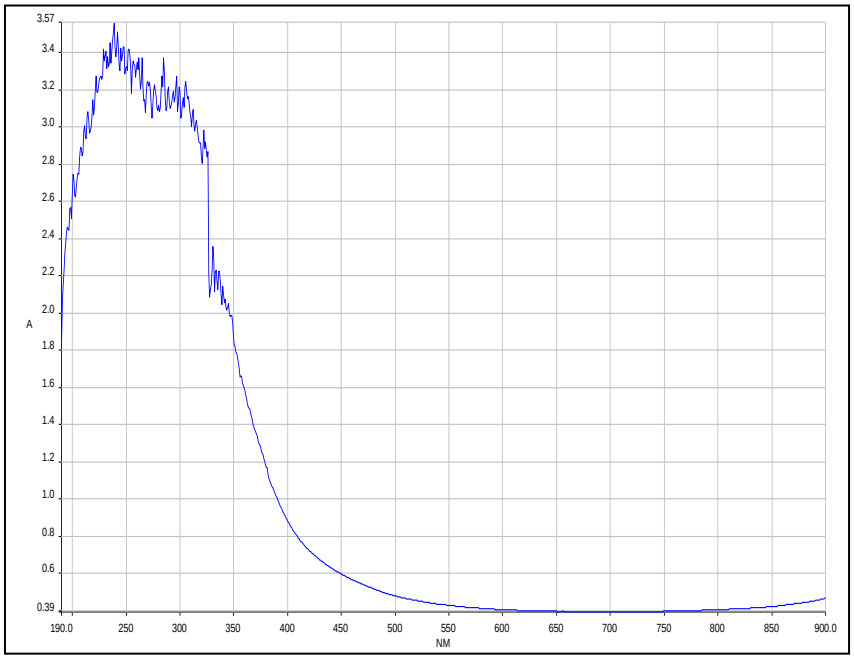

Figure 4 UV-VIS result of SiONPs produced from Bamboo

2.7. UV-VIS studies

The UV-Vis spectrum of the SiONPs spectrum synthesis from bamboo is shown in Figure. 4 as a plot of absorption versus wavelength. From the spectrum, the observed wavelength of maximum absorption for the SiONPs is between 230-300nm which indicates that the SiONPs shows a strong absorption and broader intensity in the UV region.[25] This is characteristic of silicon nanoparticles showing a successful synthetic procedure and is attributed to quantum confinement effects as well as electronic transitions associated with residual organic functional groups originating from the bamboo precursor. Typical nanoparticles like silicon based exhibiting strong UV-VIS absorption in the **230-300 nm range** are generally used for UV Protective/Blocking Coating Agent, Photocatalytic Activity and this implies more active surface sites available for interaction with heavy metals.

2.8. Adsorption studies

Adsorption kinetics plays a crucial role in predicting the rate of heavy metal ion removal from aqueous solutions. To elucidate the adsorption mechanism under varying initial concentrations and temperatures, kinetic parameters were evaluated using the pseudo-first-order model of Lagergren, based on solid-phase capacity, and the pseudo-second-order model, based on solid-phase adsorption**.** The Lagergren equation for pseudo first order kinetics can be written as follows.[26]

$$\log(q_e - q_t) = \log(q_e) - \left(\frac{k_1}{2.303}\right)t \qquad equation\ 3$$

Where q_e and q_t refers to the amount of metal ion adsorbed (mg/g) at equilibrium and at any time, t (min), respectively, and k_1(min^{-1}) is the equilibrium rate constant of pseudo first-order sorption.

From equation 3, a plot of log ($q_e - q_t$) versus t is expected to be a straight line (provided the Lagergren model is obeyed as shown in Fig. 5) with slope and intercept equal to $k_1/2.303$ and log(q_e) respectively. The Cr (VI) shows the lowest adsorption trend across all times as compared to other HMPs values. Also, a differential form of Pseudo second order kinetic model can be written as shown in equation 4 below.

$$\frac{t}{q_e} = \left(\frac{1}{k_2 q_e^2}\right) + \left(\frac{1}{q_e}\right) t \qquad \text{equation 4}$$

The implication of equation 4. is that a plot of $\frac{t}{q_e}$ versus t should be a straight line with slope and intercept being $\frac{1}{q_e}$ and $\frac{1}{k_2 q_e^2}$ respectively. Fig. 6 show kinetic plots for a Pseudo second order model. In the plot Cr (VI) shows the highest t/qt values, indicating slower adsorption kinetics, while Cd (II) exhibits moderate increase with time.

Table 3 Pseudo first and second order rate constants for the adsorption of some selected HMPs by SiONPs from bamboo

Cation	q_e (mg/g)	k_1 (min^{-1})	R^2	q_e (mg/g)	K_2 ($gmg^{-1}min^{-1}$)	R^2
Pb (II)	1.0055	0.0055	0.9278	78.1250	0.0002	0.9644
Cr (VI)	1.0051	0.0051	0.8904	25.0000	0.0013	0.9172
Cd (II)	1.0028	0.0028	0.7708	32.1543	-0.0272	0.9766

From the table 3, the correlation coefficient for a Pseudo first and second order kinetic models were found to be consistent with the adsorption of Pb (II), Cd (II) and Cr (VI) ions, with both R^2 values being closer to unity.

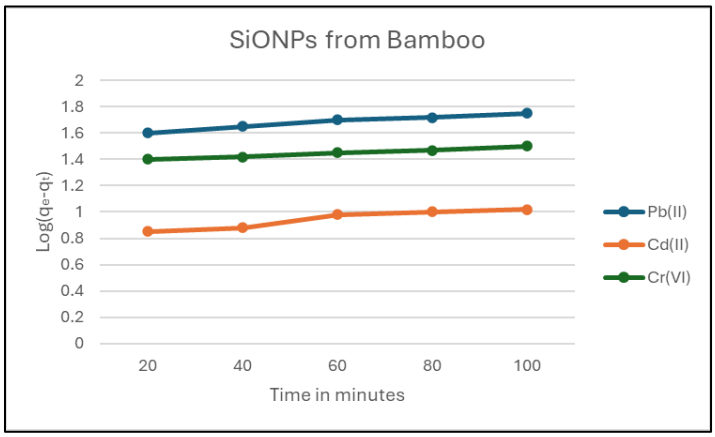

Figure 5 Variation of log ($q_e - q_t$) with t for the adsorption of some heavy metal ions by SiONPs from Bamboo

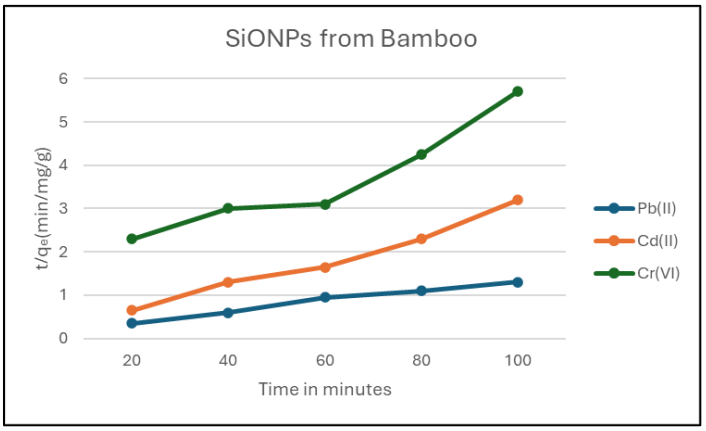

Figure 6 Variation of $\frac{t}{q_e}$ with t for the adsorption of some heavy metal ions by SiONPs from bamboo

Adsorption studies of SiONPs from bamboo was carried out at ambient temperature of (298k) in a mixer shaker water bath using 100ml conical flask as a reactor. The studies were carried out using batch adsorption method as reported elsewhere by a previous researcher.[27] The respective concentrations of the studied heavy metals before and after adsorption were determined using atomic absorption spectrophotometer (Model no AA-6800-SHIMADZU). From the measured concentrations, the amount of the metal ion adsorbed in mg was calculated using the following equation 5 below.

$$qe = \frac{MV\,(Ce - Co)}{1000} \qquad \text{equation 5}$$

where qe is the concentration of the adsorbate in mg/g of the adsorbent, C_0 and C_e are the initial concentration (before adsorption in mg/L) and equilibrium concentration (after adsorption in mg/L) of the metal ion, M is the mass of the adsorbate (in mg) and V is the volume of solution (in ml). The percentage metal ion removal (%Rem) will be calculated using the equation 6 below:

$$\%Rem = \frac{(C0 - Ce)\ X\ 100}{c_0} \qquad \text{equation 6}$$

Experimental adsorption parameters were varied to determine the effect of contact time, effect of adsorbent dose and effect of concentration of heavy metals in solution with the SiONPs. Experimental data obtained from the adsorption studies were interpreted using the Langmuir, Freundlich, Dubinin Raduskevich and Temkin isotherm models. The adsorption rate was studied using the pseudo-first order and pseudo-first order reaction models.

3. Result and discussion

3.1. Effect of contact time

The effect of contact time was investigated to determine the optimum duration required to achieve maximum adsorption. The data obtained from this study were utilized to evaluate the adsorption kinetics. At constant initial concentration, fixed adsorbent dosage, predetermined pH, and room temperature, the influence of contact time was examined by varying the agitation period. Agitation times of 20,40, 60, 80 and 100 minutes were employed for the experiment**.** From the Figure 7, it can be seen that the adsorption of lead is less dependent on time but that of cadmium and chromium shows and irregular dependent on time pattern. The period of contact of an adsorbate and SiONPs is of great importance in adsorption study because it depends on the nature of the system used. Adsorption of heavy metals unto a non-living cell is generally considered as a rapid process that occurs within 20 minute[28] as seen in the Figure 7.

It was also observed that the amount of Pb (II)ions adsorbed were higher than the amount of Cr(VI) and Cd(II) ions adsorbed, this may be as a result of higher affinity of Pb(II)ions to SiONPs.[29] Also, the amount of Cd(II) ions adsorbed displayed a decrease between 40 and 60 minutes' period of contact, this may be as a result of competitive processes such as desorption that may set in, hence the amount of ions adsorbed may decreased, explaining the drop in adsorption capacity of Cd(II) and Cr(VI) ions.[30] On the other hand, the amount of Pb (II) ions adsorbed onto the SiONPs surfaces after saturation of the adsorption sites were found to be constant with time.[31]

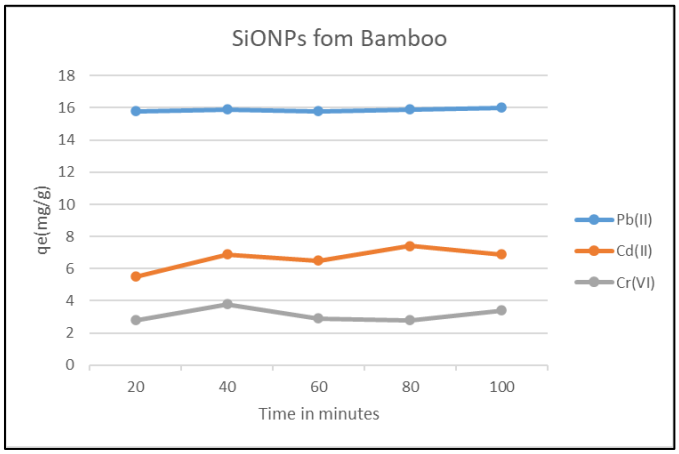

Figure 7 Variation of the amount of heavy metal ion adsorbed per unit mass of SiONPs from bamboo with time

3.2. Effect of concentration of heavy metal in solution

Figure. 8 shows plot for the variation of amount of heavy metal adsorbed (%) (per unit mass of the SiONPs from bamboo with varying concentrations of the respective heavy metal ions (i.e, Pb(II), Cr(VI) and Cd(II)ions. From the Figure 8, it is evident that the amount of heavy metal ions adsorbed per unit mass of SiONPs increases as the concentration of the heavy metal ions in the aqueous solution increase. This may be due to an increase in the rate of diffusion of the heavy metal ions to the SiONPs surface. Such increase in rate will certainly increase the sticking probability of the heavy metal as a result of the increase in the amount of adsorbate approaching the surface of the adsorbent. Again, Pb(II) ions is the highest adsorbed due to the stronger affinity of Pb(II) to SiONPs compared to other metal ions,

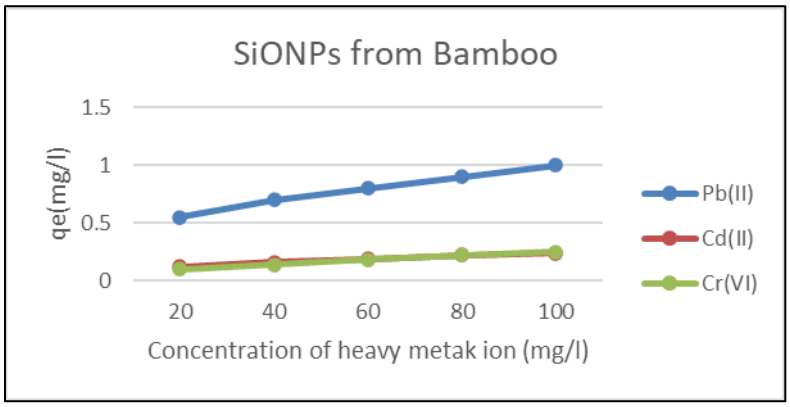

Figure 8 Variation of amount of heavy metal ion adsorbed by SiONPs from Bamboo with varying concentration of the metal ion in solution

3.3. Effect of adsorbent dose

The effect of adsorbent dose on the amount of Pb(II), Cr(VI) and Cd(II)ions removed was studied by the application of different doses ranging from 0.2 to 1.0g of the SiONPs at heavy metal concentration of 600 mg/l and at a room temperature (Figure. 9). The removal of Pb(II), Cr(VI) and Cd(II)ions was observed to be dependent on the concentration of SiONPs used in the adsorption medium; the more the adsorbent, the higher the removal efficiency.

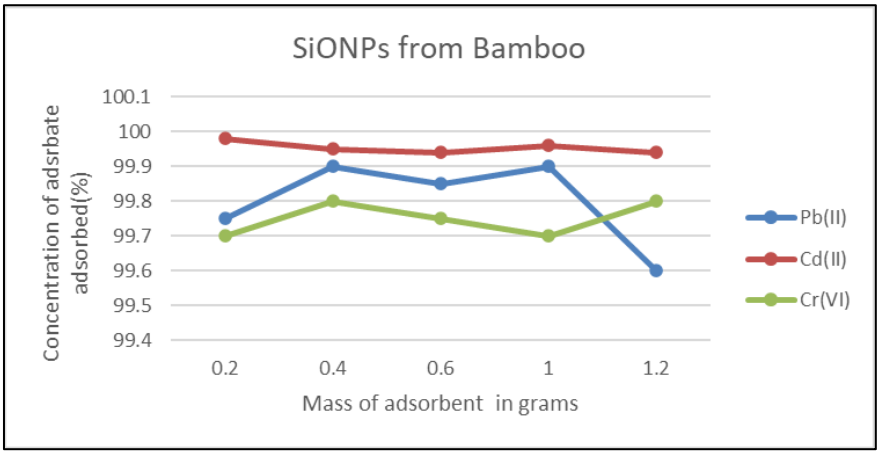

Figure 9 Variation of the concentration of adsorbed heavy metal ions with mass of the adsorbent for the adsorption of some heavy metal ions by SiONPs from bamboo

3.4. Adsorption isotherms

To optimize the adsorption performance of the three heavy metals onto SiONPs from bamboo, equilibrium data representing the amount of metal ions adsorbed per unit mass of adsorbent at varying initial concentrations were analyzed using established isotherm models, including Freundlich, and Temkin. The results indicated that the Freundlich and Temkin isotherm models provided the best fit for the adsorption behavior of SiONPs from bamboo toward Pb(II), Cr(VI) and Cd(II)ions. The equation for the Freundlich adsorption model can be written in the form given by equation 7[32]

$$q_e = kC_e^{\frac{1}{n}} \qquad \text{equation 7}$$

Where *k* and *n* are the Freundlich's constants related to the adsorption capacity and adsorption intensity of the system. If we take the logarithm of both sides, equation 7 will now become equation 8 as obtained below.

$$log(q_e) = logk + \frac{1}{n} logC_e \qquad equation\ 8$$

K and *n* can be determined from the linear plot of log q_e (Fig.10) against log C_e. $1/n$ is indicating the adsorption intensity of heavy metal ion onto the sorbent or surface heterogeneity, becoming more heterogeneous as its value gets closer to zero. A value for $1/n$ below 1 indicates a normal Freundlich isotherm while $1/n$ above 1 is indicative of cooperative adsorption. The Freundlich adsorption constants evaluated from the isotherms for Pb(II), Cr(VI) and Cd(II) ions are presented in Table 4. The adsorption data for the three investigated metal ions exhibited excellent correlation with the Freundlich isotherm model, as evidenced by high correlation coefficients (R^2) being near unity. The nearly parallel nature of the Freundlich plots suggests that the adsorption of Pb(II), Cr(VI) and Cd(II) ions onto SiONPs from bamboo proceeds via a similar mechanism. Furthermore, the calculated Freundlich intensity parameter (n) values were greater than unity for all the studied metal ions, indicating favorable adsorption and suggesting the occurrence of normal adsorption processes.[33]

The adsorption of Pb(II), Cr(VI) and Cd(II) ions by SiONPs from bamboo was also found to obey the Temkin adsorption isotherm, which can be written according to equation 9 below.

$$q_e = A + BlnC_e \qquad \text{equation 9}$$

Where q_e is the concentration of the adsorbate in mg/g of the adsorbent, B is the Temkin's constant, where *A* is the Temkin adsorption potential, and C_e(mg/l) is the equilibrium adsorbate concentrations in the solid and aqueous phases. The Temkin isotherm plots of q_e_versus lnC_e as seen in Figure. 11 showed strong linearity with high R^2 values, confirming the applicability of the Temkin-type isotherm plot. The elevated Temkin constants indicate significant adsorbate–adsorbent interactions,the values of B and R suggest strongly that Temkin model can be used to interpret the adsorption mechanism.

Table 4 Freundlich and Temkin parameters for the adsorption of some heavy metals by SiONPs from Bamboo

Metal ion	Freundlich parameters			Temkin parameters		
	1/n	logk	R^2	B	A	R^2
Pb (II)	0.1793	-6.5819	0.9472	1.3402	1.018	1.0000
C r(VI)	0.1792	-6.5904	0.9576	1.3127	1.0057	1.0000
Cd (II)	0.1794	-6.5738	0.9677	1.3023	1.0006	1.0000

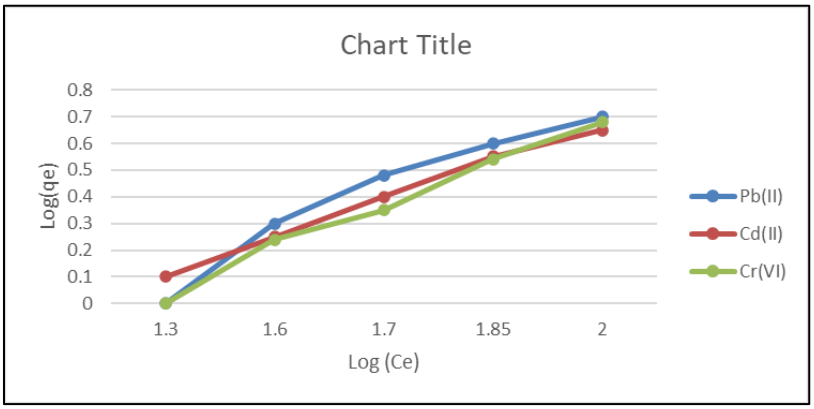

Figure 10 Variation of log(q_e) with log (C_e) for the adsorption of some heavy metals by SiONPs from bamboo

Table 5 D-R parameters for the adsorption of some heavy metals by SiONPs from bamboo

Metal ion	β(mg²/kJ²)	ln(X_m)	E (kJ/mol)	R^2
Pb(II)	0.2458	1.3914	1.4262	0.8688
Cr(VI)	0.2470	1.389	1.4228	0.8703
Cd(II)	0.2456	1.3919	1.4268	0.8692

The Dubinin–Radushkevich(D-R) isotherm is used to distinguish between chemical and physical adsorption phenomena**,** its equation is expressed as below**,**

$$lnq_e = lnX_m - \beta\left(RTln\left(1+\frac{1}{C_e}\right)\right)^2 \qquad \text{equation 10}$$

Where lnq_e(mg/g) is the concentration of the adsorbate adsorbed in the adsorbent, X_m(mg/g) is the

maximum sorption capacity, β (mg²/kJ²) is a constant related to the mean adsorption energy R (kJ/mol/K) is the gas constant and T (K) is the temperature. The bracketed terms in equation 10 represent the polanyl potential while the constant, β is related to the mean adsorption energy (E) according to the following equation,

$$E = \frac{1}{(2\beta)^{\frac{1}{2}}} \qquad \text{equation 11}$$

From equation 10, a plot of lnq_e versus $\left(RTln\left(1+\frac{1}{C_e}\right)\right)^2$ would give a straight line with slope and intercept equal to β and lnX_m respectively. Figure 12 illustrate the (D–R) isotherms for Pb(II), Cr(VI) and Cd(II) adsorption onto SiONPs from bamboo, with the corresponding parameters presented in Table 5. The calculated mean adsorption energies (E) were all below 8 kJ mol^{-1}, confirming that the uptake process is predominantly governed by Physi-sorption, characterized by weak van der Waals interactions rather than chemical bonding.

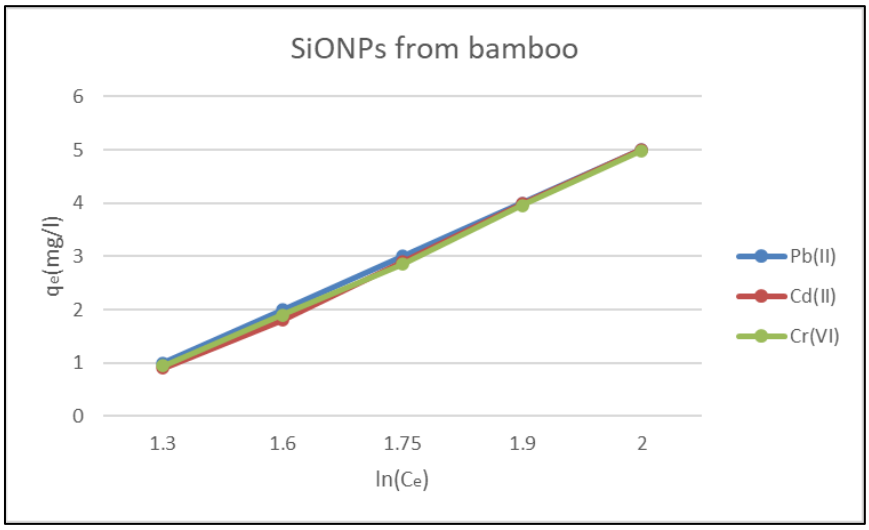

Figure 11 Variation of q_e with ln(C_e) for the adsorption of some heavy metal ions by SiONPs from bamboo

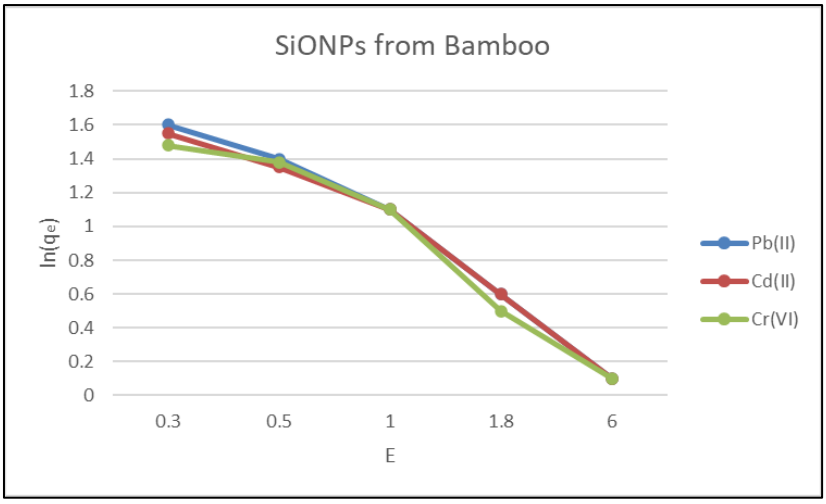

Figure 12 Variation of log(q_e) with ε for the adsorption of some heavy metal ion by SiONPs from Bamboo

3.5. Post adsorption characterization

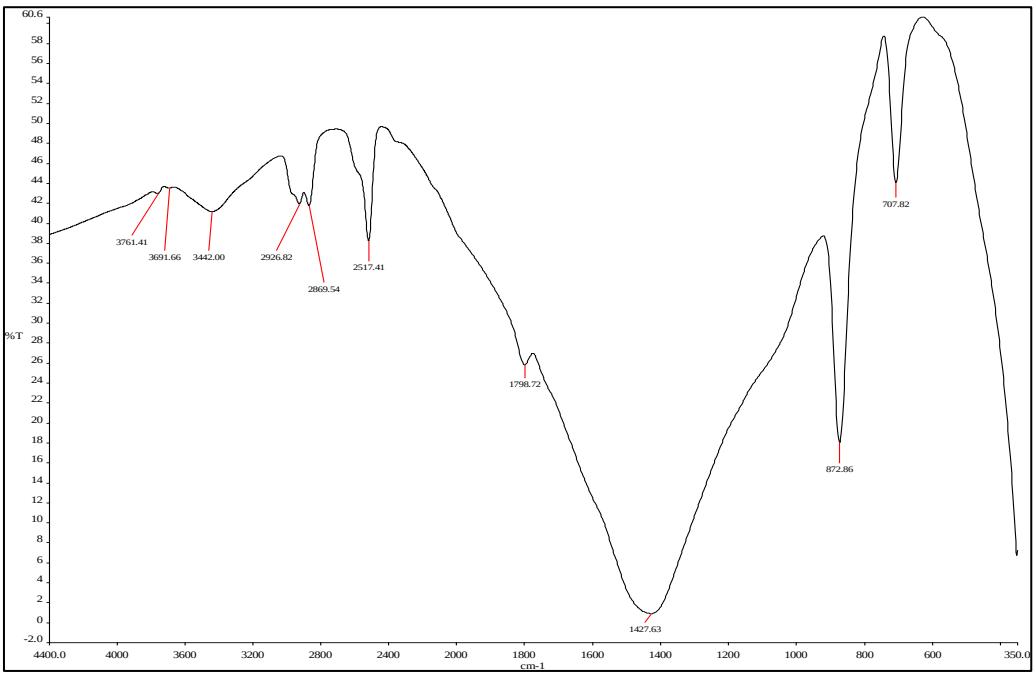

Figure 13 FTIR result of SiONPs produced from Bamboo after adsorption studies

3.6. FTIR post adsorption studies

Fourier Transform Infrared (FTIR) spectroscopy was employed to characterize the surface functional groups of bamboo-derived silicon nanoparticles (SiONPs) and to elucidate their interactions with Pb(II), Cd(II), and chromium species [Cr(VI) and Cr(II)], thereby assessing adsorption selectivity. Comparative analysis of spectra before and after adsorption provides insight into metal-specific binding mechanisms.

The pristine SiONPs exhibit a broad band at 3200–3500 cm^{-1}, attributed to –OH and Si–OH stretching vibrations, which represent the principal active sites for metal uptake. Following Pb(II) adsorption, this band shows marked intensity reduction and a shift to lower wavenumbers, indicating strong inner-sphere complexation and formation of Pb–O–Si bonds, consistent with chemisorption. In contrast, Cd(II) adsorption produces moderate peak shifts and attenuation, suggesting weaker surface complexation dominated by ion exchange and electrostatic interactions with deprotonated silanol groups.

For Cr(VI), minimal peak shifting but noticeable band broadening in the hydroxyl region is observed. Considering that Cr(VI) predominantly exists as oxyanions ($HCrO_4^-/CrO_4^{2-}$), the spectral changes indicate adsorption via electrostatic attraction to protonated silanol sites rather than direct coordination, reflecting a distinct interaction mechanism compared to divalent cations.

The carbonyl band at 1700–1735 cm^{-1}, associated with residual carboxyl groups, exhibits significant attenuation after Pb(II) adsorption, confirming its involvement in chelation, while less pronounced changes occur for Cd(II) and Cr(VI). The Si–O–Si framework bands (1000–1150 cm^{-1}) remain largely preserved after adsorption, confirming structural stability of the silica network, with slight intensity reductions most evident for Pb(II).

Overall, the extent of spectral modification follows the order Pb(II) > Cd(II) > Cr(VI), correlating with relative adsorption affinities. The results demonstrate that bamboo-derived SiONPs exhibit metal-selective adsorption governed by mechanism-dependent interactions: strong affinities for Pb(II) ions, predominantly ion exchange/electrostatic interactions for Cd(II), and pH-dependent electrostatic attraction for Cr(VI).

Table 6 XRF profiling for the oxide composition of the SiONPs from Bamboo after absorption studies

Sample	**SiO_2**	**Al_2O_3**	**Fe_2O_3**	**MnO**	**CaO**	**P_2O_5**	**K_2O**	**TiO_2**	**MgO**	**Na_2O**	**LOI**	**Ba**	**Ce**	**Rb**	**Cd**	**Cr**	**Cu**	**Cd**	**Pb**
Bamboo after Adsorption	52.54	20.85	3.65	0.01	1.94	-	0.95	1.17	0.08	0.05	0.20	0.46	0.58	0.95	0.70	5.5	0.35	0.40	10

3.7. XRF post adsorption studies.

X-ray fluorescence (XRF) analysis was conducted to determine the elemental composition of bamboo-derived silicon nanoparticles (SiNPs) after heavy metal adsorption. The results indicate that SiO_2 remains the dominant oxide (52.54 wt%), confirming preservation of the silica-rich framework and structural stability of the adsorbent following adsorption. Significant amounts of Al_2O_3 (20.85 wt%) and Fe_2O_3 (3.65 wt%) were also observed, suggesting the persistence of aluminosilicate and iron-containing phases that may enhance adsorption through additional surface hydroxyl groups and active binding sites. Minor oxides, including TiO_2, CaO, K_2O, MgO, and Na_2O, reflect the inherent mineral composition of the bamboo precursor and contribute to surface heterogeneity.

Post-adsorption analysis reveals notable accumulation of heavy metals, particularly Pb (10.0 wt%) and Cr (5.50 wt%), alongside Cd and Cu in lower concentrations, confirming effective metal uptake and immobilization on the SiNP surfaces. The pronounced Pb content indicates strong affinity, likely mediated by electrostatic interactions and surface complexation with silanol groups. Trace elements (Ba, Ce, and Rb) were also detected, suggesting broad-spectrum adsorption capability. The low loss on ignition (0.20 wt%) further indicates minimal residual organics and good thermal stability. Overall, the findings confirm that bamboo-derived SiNPs retain structural integrity while demonstrating high adsorption efficiency and suitability for wastewater remediation applications.

3.8. SEM-EDX post adsorption studies

The SEM-EDX post absorption characterization as shown in Figure 14 marks notable changes observed in the EDX spectrum as compared to the pre-adsorption SEM-EDX observed in Figure. 2. Silicon remains the dominant element having the highest atomic percentage(68.80 at.%), suggest that adsorption studies with heavy metals does not disrupt the silicon-rich framework of the nanoparticles, this further highlights the structural stability and reactivity of the bamboo-derived silicon nanoparticles. A clear increase in carbon and oxygen atomic percentages(3.02 at.% and 13.74 at%) indicates interaction and accumulation of organic pollutants (dyes, pesticides, oils) on the adsorbent's surface and the presence of oxygen-containing functional groups[35] suggesting that apart from heavy metals, silicon nanoparticles can find applications in removal of dyes, pesticides and oils.

The detection of Pb (0.60 at.%), Cr (0.20 at.%), and Cd (0.10 at.%), by post SEM-EDX characterization which were completely absent before adsorption, provides strong confirmation of successful and selective immobilization of these three heavy metals onto the silicon nanoparticle surface. The detection of these metals verifies the potentials of bamboo-derived silicon nanoparticles as adsorbents for toxic metal remediation.

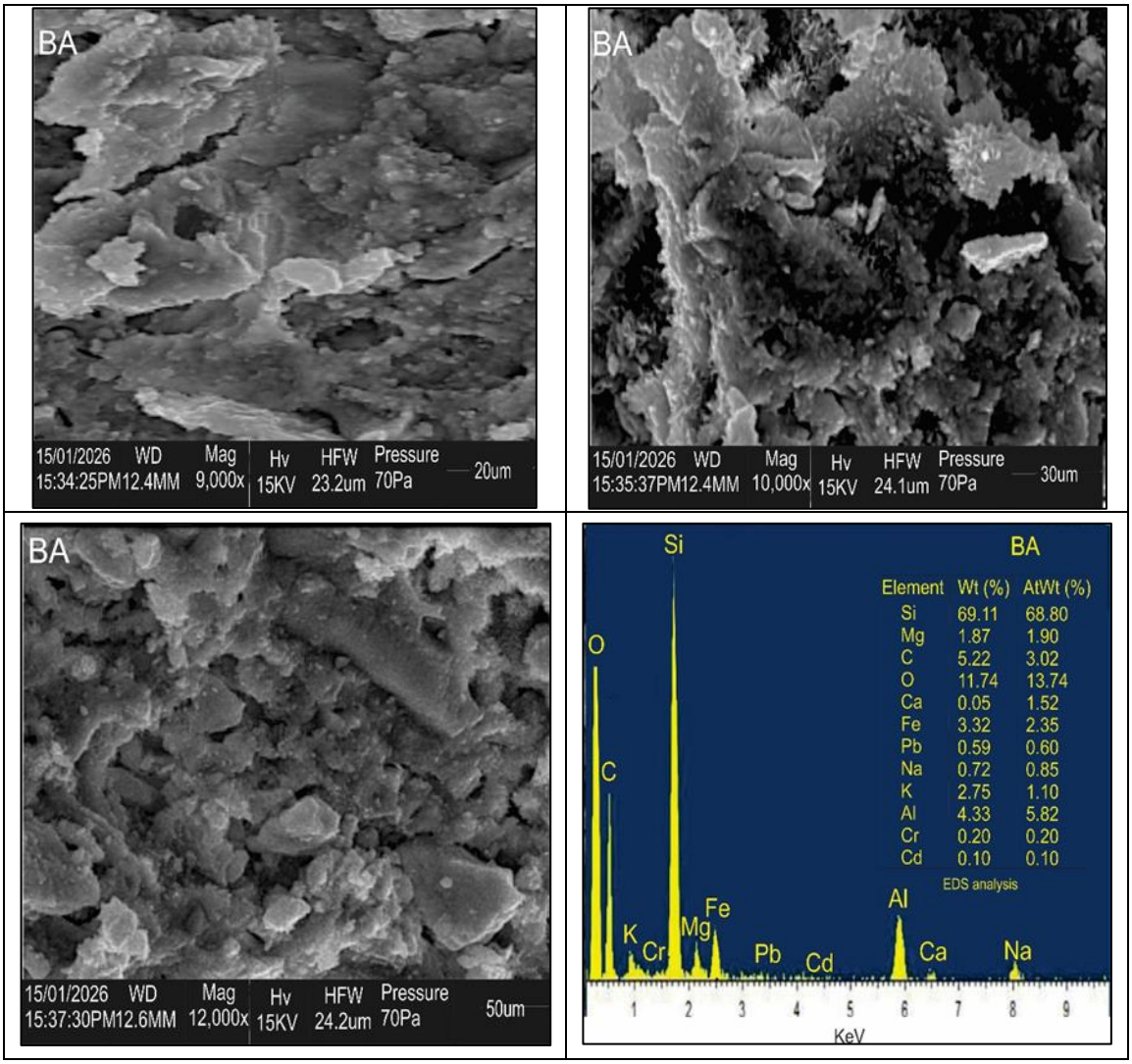

Figure 14 SEM-EDX result of SiONPs produced from Bamboo after adsorption studies

The increased presence of Fe (2.35 at.%), Al (5.82 at.%), and alkali/alkaline earth metals (Na, K, Ca, Mg) after adsorption further suggests that ion exchange, surface complexation, and possible chelating potentials[36] of silicon nanoparticles contribute to metal uptake. The coexistence of these elements may enhance adsorption by creating heterogeneous active sites and facilitating electrostatic interactions.

These results strongly support their suitability of silicon nanoparticles derived from bamboo as low-cost, biomass-derived adsorbents for the remediation of heavy-metal in contaminated water.

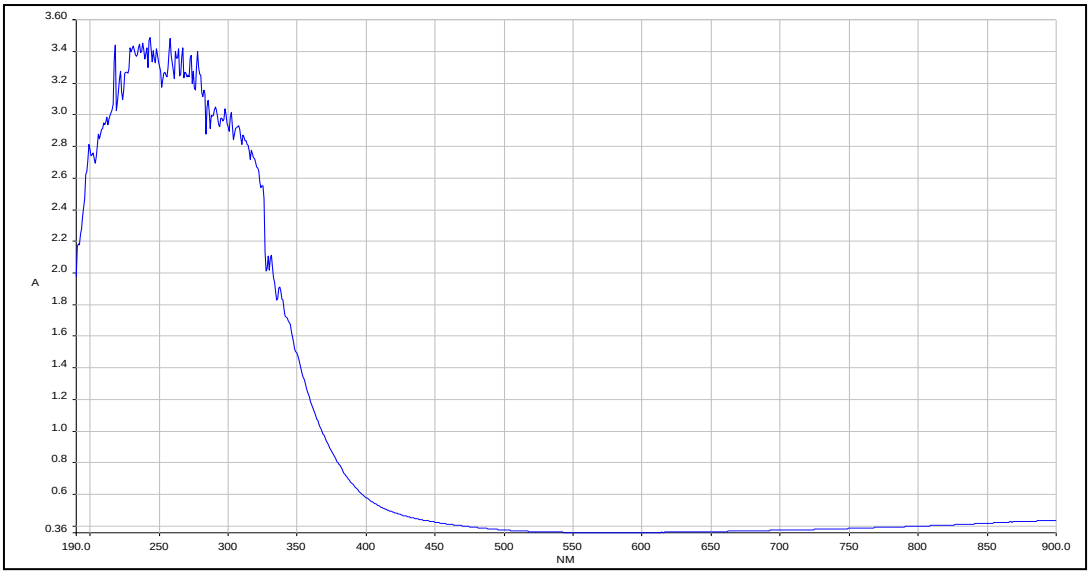

Figure 15 UV-VIS result of SiONPs produced from Bamboo after adsorption studies

3.9. The UV-VIS post adsorption studies

The UV-VIS post adsorption studies clearly demonstrate a reduced absorbance intensity in the UV region together with a slight red shift and smoothing of the absorption edge. These spectral changes are indicative of successful adsorption of the target heavy metal species onto the surface of the silicon nanoparticles. The reduction in absorbance intensity can be attributed to surface coverage and partial passivation of active sites, while the red shift suggests electronic interaction between the adsorbed molecules and the silicon nanoparticle surface, possibly resulting in an increase in effective particle size or modification of surface energy states due to adsorption. Overall, the observed changes in the UV–Vis spectra after adsorption studies provide strong evidence of adsorption-induced modification of the optical properties of bamboo-derived silicon nanoparticles making the adsorbent excellent for various application. The interaction between the adsorbate and the silicon nanoparticle surface alters the electronic structure to stability and confirms the effectiveness of the adsorption process.

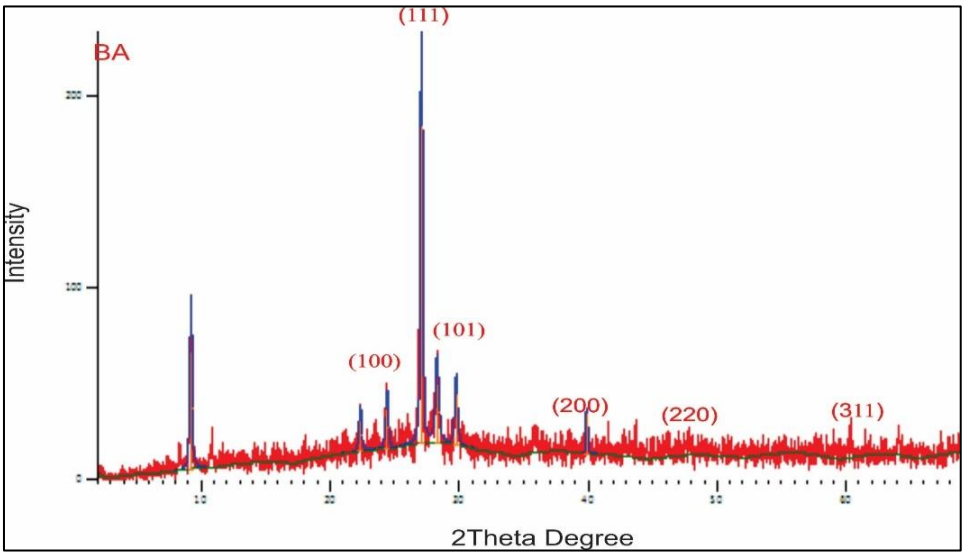

Figure 16 XRD result of SiONPs produced from Bamboo after adsorption studies

3.10. XRD post adsorption

The X-ray diffraction (XRD) pattern of bamboo-derived silicon nanoparticles after heavy metal adsorption is presented in Figure 16. The diffractogram exhibits distinct diffraction peaks indexed to the (100), (101), (111), (200), (220), and

(311) crystallographic planes, confirming that the crystalline structure of the silicon nanoparticles is largely retained following the adsorption process.

The prominent diffraction peak observed at approximately 2θ ≈ 28–29°, corresponding to the (111) plane, remains the most intense reflection after adsorption. This indicates that the adsorption of heavy metal ions onto the nanoparticle surface does not significantly disrupt the intrinsic crystal lattice of the silicon phase. The persistence of this dominant peak suggests good structural stability of the bamboo-derived silicon nanoparticles during the adsorption process, which is essential for their reusability in environmental remediation applications.

Compared with the XRD pattern before adsorption as shown in Figure 1, a noticeable reduction in peak intensity and slight peak broadening are observed for several reflections, particularly those corresponding to the (100) and (101) planes. These changes can be attributed to the interaction of heavy metal ions with surface functional groups and active sites on the silicon nanoparticles, leading to partial surface coverage and increased lattice strain. Such effects are commonly reported in adsorption studies and are indicative of successful metal ion binding onto the adsorbent surface.

Additionally, the elevated background intensity and broadened baseline observed across the diffractogram suggest an increase in the amorphous content after adsorption. This behavior is associated with the deposition of heavy metal species and possible formation of metal–oxygen or metal–silicon complexes on the nanoparticle surface. The absence of new sharp diffraction peaks corresponding to crystalline metal or metal oxide phases indicates that the adsorbed heavy metals are predominantly present in an amorphous or highly dispersed state rather than forming bulk crystalline compounds.

No extra diffraction peaks associated with secondary impurity phases are detected, confirming that the adsorption process does not induce phase transformation or structural degradation of the silicon nanoparticles. The retention of the original crystal structure, coupled with subtle intensity variations, confirms that adsorption occurs mainly through surface interactions rather than bulk lattice incorporation.

Overall, the XRD results demonstrate that bamboo-derived silicon nanoparticles maintain their crystalline integrity after heavy metal adsorption, while the observed peak intensity reduction and background broadening provide strong evidence of successful adsorption. These structural features highlight the suitability of the synthesized nanoparticles as stable and effective adsorbents for heavy metal removal from contaminated water.

4. Conclusion

The results of the study revealed that silicon nanoparticles synthesized from bamboo stem are excellent adsorbents for the studied metal ions. These adsorbents adsorbed functions through the mechanism of physical adsorption since the extent of adsorption increases with increasing metal ion concentrations and adsorption is time independent. The adsorption properties of these adsorbents fitted a pseudo first order kinetics while its characteristics was best described by Freundlich, Temkin and Dubinin-Radushkevich adsorption isotherm. Adsorption parameters deduced from these isotherms indicated the presence of strong interaction between the adsorbate and the adsorbent and the existent of the mechanism of physical adsorption.

Compliance with ethical standards

Acknowledgments

The authors thank the Tertiary education trust fund for the award of the 2025 Institutional based research (IBR) sponsoring this research work.

Disclosure of conflict of interest

The authors state that there is no conflict of interest to declare.

Data availability statement

Data associated with this work are available in the manuscript

References

[1] Federal Ministry of Environment. National Policy on the Environment (Revised 2016). Policy Rev. 1–58 (2016).

[2] Awual, M. R., Yaita, T. and Okamoto, Y. A novel ligand based dual conjugate adsorbent for cobalt(II) and copper(II) ions capturing from water. Sensors Actuators, B Chem. 203, 71–80 (2014).

[3] Impacts, H. and Remediation, M. Water Quality Degradation Due to Heavy Metal Contamination : Health Impacts and Eco-Friendly Approaches for Heavy. (2023).

[4] Bai, M. et al. Occurrence and Health Risks of Heavy Metals in Drinking Water of Self-Supplied Wells in Northern China. Int. J. Environ. Res. Public Health 19, (2022).

[5] Farooq, U., Kozinski, J. A., Khan, M. A. and Athar, M. Biosorption of heavy metal ions using wheat based biosorbents - A review of the recent literature. Bioresource Technology vol. 101 5043–5053 at https://doi.org/10.1016/j.biortech.2010.02.030 (2010).

[6] Kobielska, P. A., Howarth, A. J., Farha, O. K. and Nayak, S. Metal–organic frameworks for heavy metal removal from water. Coordination Chemistry Reviews vol. 358 92–107 at https://doi.org/10.1016/j.ccr.2017.12.010 (2018).

[7] Huang, H. et al. Graphitic carbon nitride solid nanofilms for selective and recyclable sensing of Cu2+ and Ag+ in water and serum. Chem. Commun. 50, 15415–15418 (2014).

[8] Schwarzenbach, R. P., Egli, T., Hofstetter, T. B., Von Gunten, U. and Wehrli, B. Global water pollution and human health. Annu. Rev. Environ. Resour. 35, 109–136 (2010).

[9] Guo, X. Y. et al. Geochemistry Process from Weathering Rocks to Soils: Perspective of an Ecological Geology Survey in China. Sustain. 15, 1–20 (2023).

[10] Wu, T. et al. Amidoxime-Functionalized Macroporous Carbon Self-Refreshed Electrode Materials for Rapid and High-Capacity Removal of Heavy Metal from Water. ACS Cent. Sci. 5, 719–726 (2019).

[11] Barakat, M. A. New trends in removing heavy metals from industrial wastewater. Arabian Journal of Chemistry vol. 4 361–377 at https://doi.org/10.1016/j.arabjc.2010.07.019 (2011).

[12] Khezami, L. and Capart, R. Removal of chromium(VI) from aqueous solution by activated carbons: Kinetic and equilibrium studies. J. Hazard. Mater. 123, 223–231 (2005).

[13] Naseem, R. and Tahir, S. S. Removal of Pb(II) from aqueous/acidic solutions by using bentonite as an adsorbent. Water Res. 35, 3982–3986 (2001).

[14] Jaishankar, M., Tseten, T., Anbalagan, N., Mathew, B. B. and Beeregowda, K. N. Toxicity, mechanism and health effects of some heavy metals. Interdisciplinary Toxicology vol. 7 60–72 at https://doi.org/10.2478/intox-2014-0009 (2014).

[15] Paulino, A. T. et al. Novel adsorbent based on silkworm chrysalides for removal of heavy metals from wastewaters. J. Colloid Interface Sci. 301, 479–487 (2006).

[16] Singh, V., Mondal, P. C., Singh, A. K. and Zharnikov, M. Molecular sensors confined on SiOx substrates. Coord. Chem. Rev. 330, 144–163 (2017).

[17] Hu, Y. et al. Assessing heavy metal pollution in the surface soils of a region that had undergone three decades of intense industrialization and urbanization. Environ. Sci. Pollut. Res. 20, 6150–6159 (2013).

[18] Manandhar, R., Kim, J. H. and Kim, J. T. Environmental, social and economic sustainability of bamboo and bamboo-based construction materials in buildings. J. Asian Archit. Build. Eng. 18, 52–62 (2019).

[19] Kolawole, I. D. et al. Economic impact of waste from food, water, and agriculture in Nigeria: challenges, implications, and applications—a review. Discov. Environ. 2, (2024).

[20] Khan, M. et al. Mechanistic breakthroughs in affordable adsorbents for heavy metal remediation: An in-depth exploration of next-generation sustainable water purification technologies. J. Hazard. Mater. Adv. 19, 100847 (2025).

[21] Ortega-Toro, R., Villabona-Ortíz, Á., Tejada-Tovar, C., Herrera-Barros, A. and Cabrales-Sanjuan, D. Use of Sawdust (Aspidosperma polyneuron) in the Preparation of a Biocarbon-Type Adsorbent Material for Its Potential Use in the Elimination of Cationic Contaminants in Wastewater. Water (Switzerland) 15, (2023).

[22] Essien, N. B. Rice Husk as Precursor for Silicon Oxide Nanoparticles : Synthesis and Characterization. 11, (2024).

[23] Farirai, F. et al. Methods of extracting silica and silicon from agricultural waste ashes and application of the produced silicon in solar cells: a mini-review. Int. J. Sustain. Eng. 14, 57–78 (2021).

[24] Shanaz, A., Abdulgalim, I., Richard, S., Ilya, P. and Valery, T. Removal of Copper (II) from Aqueous Solutions Using Silica Xerogel as Sorbent: Adsorption Properties and Mechanism. Colloids and Interfaces 9, 1–17 (2025).

[25] Bols, M. L. et al. In Situ UV-Vis-NIR Absorption Spectroscopy and Catalysis. Chem. Rev. 124, 2352–2418 (2024).

[26] Revellame, E. D., Fortela, D. L., Sharp, W., Hernandez, R. and Zappi, M. E. Adsorption kinetic modeling using pseudo-first order and pseudo-second order rate laws: A review. Clean. Eng. Technol. 1, 100032 (2020).

[27] Essien, N. B. Maize Waste Biomass as an Adsorbent for the Removal of Pb2+, Zn2+ and Cu2+ from Aqueous Solution. Chem. Res. J. 3, 34–44 (2018).

[28] Raji, Z., Karim, A., Karam, A. and Khalloufi, S. Adsorption of Heavy Metals : Mechanisms , Kinetics , and Applications of Various Adsorbents in Wastewater Remediation — A Review. 775–805 (2023).

[29] El-shafey, S. E., Obada, M. K. and Mohamed, W. S. Silica / klucel nanocomposite as promising durable adsorbent for lead removal from industrial effluents. 1–17 (2024).

[30] Mohamed, H. S. et al. Adsorption of Cd 2 D and Cr 3 D ions from aqueous solutions by using residue of Padina gymnospora waste as promising low-cost adsorbent. Heliyon e01287 (2019) doi:10.1016/j.heliyon.2019.e01287.

[31] Xu, Y. et al. Study on Efficient Adsorption Mechanism of Pb 2 + by Magnetic Coconut Biochar. (2022).

[32] State, K., State, E. and State, K. Langmuir , Freundlich , Temkin and Dubinin – Radushkevich Isotherms Studies of Equilibrium Sorption of Zn 2 + Unto Phosphoric Acid Modified Rice Husk. 3, 38–45 (2012).

[33] Essien, N. and E. N. ADSORPTION OF LEAD AND CHROMIUM IONS FROM AQUEOUS SOLUTION USING SORGHUM WASTE. Int. J. Eng. Res. A Peer Rev. Int. J. Vol.3., 662–672 (2015).

[34] Dai, J., Ren, F. L. and Tao, C. Adsorption of Cr(VI) and speciation of Cr(VI) and Cr(III) in aqueous solutions using chemically modified chitosan. Int. J. Environ. Res. Public Health 9, 1757–1770 (2012).

[35] Kibami, D., Pongener, C., Rao, K. S. and Sinha, D. Surface characterization and adsorption studies of Bambusa vulgaris-a low cost adsorbent. J. Mater. Environ. Sci. 8, 2494–2505 (2017).

[36] Jurkowski, W., Paper, M. and Brück, T. B. Isolation and Investigation of Natural Rare Earth Metal Chelating Agents From Calothrix brevissima - A Step Towards Unraveling the Mechanisms of Metal Biosorption. Front. Bioeng. Biotechnol. 10, 1–10 (2022).